nature communications

Article

https://doi.org/10.1038/s41467-025-67986-w

Aldehyde cool-flame chemistry explains a missing source of organic acids

Received: 9 June 2025

Accepted: 15 December 2025

Published online: 26 December 2025

Check for updates

Bingzhi Liu[1], Bin Dong[1], Huanhuan Wang[1], Shanshan Ruan[1], Qingbo Zhu[1], Weiye Chen[1], Liuyuan Wang[1], Long Zhu[1], Lili Xing[2], Donald G. Truhlar[3] ✉ & Zhandong Wang[1] ✉

Combustion emission is a significant source of organic acids, impacting atmospheric chemistry and climate. Their formation mechanisms, however, remain poorly understood, leading to underestimation in kinetic models. We investigate the cool-flame oxidation of key combustion intermediates—C_1–C_4 aldehydes and benzaldehyde. Using in-situ synchrotron vacuum ultraviolet photoionization mass spectrometry, we observe the direct conversion of aldehydes to organic acids, a process enhanced by HO_2 radicals. Quantum chemistry calculations reveal that the reaction of $RC(O)O_2$ with HO_2 on the singlet potential energy surface contributes to organic acids. Incorporating this pathway into a kinetic model significantly improves organic acid prediction. Despite the high-temperature nature of engine combustion, significant spatial and temporal inhomogeneities (e.g., near-wall regions and crevice volumes) lead to localized cool-flame conditions, facilitating organic acid formation and emission. Elucidating the acid formation under cool-flame conditions provides a critical mechanism for accurately modelling anthropogenic organic acid emissions and developing mitigation strategies.

Organic acids are ubiquitous in atmospheric aerosols and are found in both the gaseous and particle phases of the atmosphere. Organic acids in aerosols have been shown to make a significant contribution to the cloud condensation nuclei (CCN) and the acidity of clouds and rainwater[1,2]. Organic acids in the atmosphere come from a variety of sources, including natural and anthropogenic, such as the degradation of volatile organic compounds (VOCs) released by plants[2,3], vehicular emissions, and biomass burning of wildfires[4–6]. Large-scale wildfires may develop extensive extreme fire behaviors[5], such as fire whirls[7,8], due to multi-flame merging[9]. The intense combustion associated with these extreme fire behaviors can decompose and generate substantial amounts of organic acids, including formic acid and acetic acid, which are directly emitted into the atmosphere, significantly increasing the direct emissions of organic acids.

In urban environments, vehicle emissions and fossil fuel combustion are important sources of organic acids in the atmosphere[10–12]. Studies on the gas-phase pollutants emitted from vehicle emissions demonstrated the presence of significant amounts of organic acids in both diesel and gasoline engine combustion[12–16]. Organic acid emissions account for 4–27% of hydrocarbon emissions from engines, 1.2–10 times higher than aldehyde emissions[14]. The fuel-based and mileage-based emission factors from 31 vehicles under different stages of emission standards highlight the significant emission of organic acids from diesel vehicles, with the emission factors of formic acid being 130 ± 134 mg/kg_{fuel}[16]. Considering the huge number of motor vehicles worldwide (the total vehicle population exceeded 1.4 billion in 2023[17]) and the rising consumption of fossil fuels, combustion is an important source of organic acids. Therefore, it is crucial to elucidate

[1]State Key Laboratory of Fire Science, and National Synchrotron Radiation Laboratory, University of Science and Technology of China, Hefei, Anhui 230026, PR China. [2]Energy and Power Engineering Institute, Henan University of Science and Technology, Luoyang 471003 Henan, PR China. [3]Department of Chemistry, Chemical Theory Center, and Minnesota Supercomputing Institute, University of Minnesota, Minneapolis, MN 55455-0431, USA. ✉e-mail: truhlar@umn.edu; zhdwang@ustc.edu.cn

the formation mechanism of organic acids during engine combustion. While engine combustion is predominantly high-temperature chemistry, substantial gradients in temperature and species concentrations arise due to wall heat transfer, flow inhomogeneities, and geometric constraints[18,19]. These regions (such as the squish area and near-wall zones) often exhibit low temperatures conducive to cool-flame chemistry, where partial oxidation of fuel-derived intermediates (e.g., aldehydes) occurs[18,19]. Furthermore, in such regions, even though some radical species may be present, they are insufficient to fully oxidize the intermediates produced during low-temperature ignition and cool-flame reactions. These zones thus serve as important sources of emission precursors[18], including organic acids, which persist into the exhaust system.

To explain the formation of organic acids, two mechanisms were proposed and adopted in the combustion models in the literature. Hydroxyl radical (OH) addition to the C = O bond of aldehydes and the subsequent bond dissociation of the adduct is one pathway for organic acid formation[20,21], e.g., the pathway of $CH_2O + OH \rightarrow HOCH_2O$ (adduct) → formic acid + H. However, this reaction pathway was found to be negligible compared to the H-atom abstraction reaction of aldehydes by hydroxyl radicals[22]. The Korcek decomposition of the cool-flame chain-branching intermediate, γ-ketohydroperoxides (γ-KHP), is a potential formation pathway of organic acids[23–25]; the Korcek pathways of γ-KHP form cyclic peroxides, which decompose to carbonyl products and organic acids[23]. The Korcek pathways of γ-KHP are dominant over the O-O bond dissociation of γ-KHP at temperature below 400 K, but become less important at typical cool-flame temperatures above 500 K. Although including the Korcek pathways of γ-KHP in combustion models enhanced the formation of organic acids, a large gap between model prediction and experimental measurements still exists[26]. For example, during the cool-flame reactions of methane and ethane, no γ-KHP was formed but formic acid and acetic acid were formed[27], suggesting that organic acids may be formed through other pathways[28].

Here, we report studies of the cool-flame reactions of typical aldehydes (formaldehyde, acetaldehyde, propanal, *n*-butanal, *iso*-butanal, and benzaldehyde) by synchrotron vacuum ultraviolet photoionization mass spectrometry (SVUV-PIMS). We observed the formation of organic acids with the same carbon skeleton as the aldehydes. The experimental measurements and quantum chemistry calculations indicate that the reaction of carbonyl peroxy radicals ($RC(O)O_2$) with HO_2 is a missing source of organic acids in cool-flame reactions. Adding these pathways to combustion models significantly promotes the formation of organic acids.

Results

Cool-flame reactions of aldehydes

The cool-flame reactions of formaldehyde and acetaldehyde were studied in a jet-stirred reactor, where the mixture of aldehyde/O_3/O_2/Ar underwent autoxidation reaction. The experimental conditions are presented in Supplementary Table S1. During the reaction, O_3 starts to decompose and produce O atoms when the temperature is above 400 K. Hydrogen abstraction from the aldehyde by an O atom forms an acyl radical, which reacts with O_2 to form a carbonyl peroxy radical, $RC(O)O_2$. Below we present SVUV-PIMS measurements of the key reaction intermediates and quantum chemistry calculations of the reaction pathways showing that the reaction of $RC(O)O_2$ with HO_2 radical yields an organic acid.

The mass spectrum of the cool-flame reaction of formaldehyde at 520 K is presented in Fig. 1a; the photon energy for the ionization is 11.5 eV. The photoionization efficiency (PIE) spectra of hydrogen peroxide[29] (*m/z* 34.01) and formic acid[30] (*m/z* 46.01) in Fig. 1b and c are used to identify two weak peaks shown in black in Fig. 1a. This shows that the cool-flame reaction of formaldehyde yields formic acid. We interpret the production of H_2O_2 as arising from bimolecular association of HO_2, implying that HO_2 radicals are also formed. This then suggests the reaction pathway in Fig. 1d, whereby the H-abstraction of CH_2O forms HCO radical, which reacts with O_2 to form $HC(O)O_2$, which reacts with HO_2 to form formic acid.

To provide further evidence for this mechanism, we studied the cool-flame reaction of methanol (CH_3OH) under conditions similar to those used for formaldehyde. CH_2O is the dominant product for the cool-flame reaction of CH_3OH, as shown in the red mass spectrum in Fig. 1a. The inferred mechanism is shown in the last line of Fig. 1d, where the H-abstraction of CH_3OH by O atom forms CH_2OH radical, which reacts with O_2 and yields CH_2O and HO_2 radical. As discussed in the previous paragraph, the cool-flame reaction of CH_2O can form $HC(O)O_2$ radical. The mass peaks corresponding to hydrogen peroxide (H_2O_2) and formic acid (HC(O)OH) are also observed. As compared to the mass spectrum for the cool-flame reaction of CH_2O, the signal intensity of H_2O_2 and HC(O)OH is much higher. The former can be explained by the O_2 addition reaction of CH_2OH radical forming a large amount of HO_2 radical, which promotes the formation of H_2O_2. The latter can be explained by the higher concentration of HO_2 radical, which further promotes its reaction with $HC(O)O_2$ radical and enhances the formation of HC(O)OH.

Figure 2a presents the mass spectrum for the cool-flame reaction of acetaldehyde at 520 K. Again, the photon energy for the ionization is 11.5 eV. In addition to the mass peak of the reactant CH_3CHO (*m/z* 44.03), we observe CH_2O at *m/z* 30.01, CH_3OH at *m/z* 32.03, H_2O_2 at *m/z* 34.01, HC(O)OH at *m/z* 46.01, CH_3O_2H at *m/z* 48.02, and $CH_3C(O)OH$ at *m/z* 60.02. The PIE spectra of methyl hydroperoxide[31] and acetic acid[28] are used to identify these products, as shown in Fig. 2b, c. This experiment shows that the cool-flame reaction of acetaldehyde forms acetic acid.

Because we showed above that the cool-flame reaction of CH_3OH forms a large amount of HO_2 radical that enhances the formation of formic acid, we added CH_3OH to the cool-flame reaction of acetaldehyde to reveal its effect on the formation of acetic acid. The reaction sequence for generating $RC(O)O_2$ and HO_2 radicals in this case is as follows:

$$O_3 \rightarrow O_2 + O \quad \text{(R1)}$$

$$RCHO + O \rightarrow RCO + OH \quad \text{(R2)}$$

$$RCO + O_2 \rightarrow RC(O)O_2 \quad \text{(R3)}$$

$$CH_3OH + O \rightarrow CH_2OH + OH \quad \text{(R4)}$$

$$CH_2OH + O_2 \rightarrow CH_2O + HO_2 \quad \text{(R5)}$$

The mass spectrum after adding 0.125% CH_3OH is presented in Fig. 2a and is compared with the mass spectrum of acetaldehyde; we see that the formation of CH_2O, H_2O_2, HC(O)OH, CH_3O_2H, and $CH_3C(O)OH$ is enhanced. Figure 2d compares the mole fraction of $CH_3C(O)OH$ formed during the cool-flame reaction of acetaldehyde to that for the cool-flame reaction of acetaldehyde + CH_3OH at 400–600 K; we see that the promotion of $CH_3C(O)OH$ by adding 0.125% CH_3OH occurs at all the studied temperatures. At the fixed temperature of 520 K, we varied the amount of added CH_3OH; Fig. 2e shows that the formation of acetic acid increases with increasing CH_3OH concentration. These results confirm that HO_2 radical is related to the formation of acetic acid and that increasing the concentration of HO_2 promotes the formation of acetic acid.

Figure 2f summarizes the mechanistic conclusions from the acetaldehyde experiments. The abstraction of H from acetaldehyde by an O atom forms a CH_3CO radical. Along one path, its decomposition

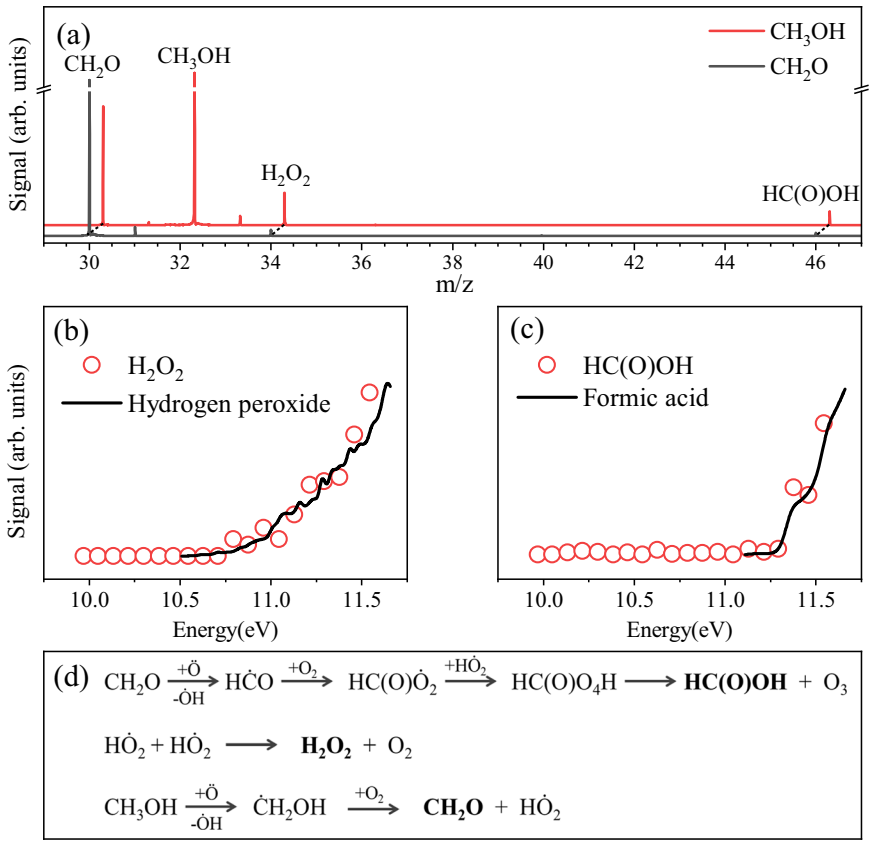

Fig. 1 | Cool-flame chemistry of CH_2O and CH_3OH. a Mass spectrum of the cool-flame reactions of CH_2O and CH_3OH recorded by synchrotron vacuum ultraviolet photoionization mass spectrometry (SVUV-PIMS) at 520 K with a photon energy of 11.5 eV. Black line: the experimental spectra of the cool-flame reactions of CH_2O; Red line: the experimental spectra of the cool-flame reactions of CH_3OH. **b**, **c** H_2O_2 and HC(O)OH product identification by comparing the photoionization efficiency (PIE) spectra of hydrogen peroxide[29] and formic acid[30]. Red symbols: the experimental PIE spectra measured in this work; Black lines: the reference PIE spectra from the literature (hydrogen peroxide[29] and formic acid[30]). **d** Reaction pathway of the cool-flame reaction of formaldehyde and methanol. The characteristic products (HC(O)OH, H_2O_2 and CH_2O) formed through the pathway are highlighted in bold.

leads to CH_3 radical and CO. The reaction of CH_3 radical with O_2 forms CH_3O_2 radical. The reaction of CH_3O_2 with HO_2 leads to CH_3O_2H, and the self-reaction of CH_3O_2 leads to CH_2O and CH_3OH. As shown in Fig. 1a, the appearance of CH_2O and CH_3OH contributes to the formation of HC(O)OH. Thus, this reaction channel explains the formation of CH_2O, CH_3OH, HC(O)OH, and CH_3O_2H. Along another path, the reaction of CH_3CO radical with O_2 leads to carbonyl peroxy radicals $CH_3C(O)O_2$. Like $HC(O)O_2$ radical, the reaction of $CH_3C(O)O_2$ with HO_2 radical leads to acetic acid ($CH_3C(O)OH$). When CH_3OH is added to the reaction system, the cool-flame reaction of CH_3OH directly leads to CH_2O and HO_2, and it also promotes the formation of formic acid. The increased concentration of HO_2 radicals further promotes the formation of H_2O_2, CH_3O_2H, and $CH_3C(O)OH$, as shown in Fig. 2a.

We also studied the cool-flame reaction of propanal, *n*-butanal, *iso*-butanal, and benzaldehyde; the experimental conditions are presented in Supplementary Table S1. Supplementary Fig. S1 shows the mass spectra and PIE spectra, which reveal that propanoic acid, butanoic acid, isobutyric acid, and benzoic acid, respectively, are formed in these experiments. This confirms that organic acids are the common reaction product of cool-flame aldehyde reactions. The inferred source is the reaction of carbonyl peroxy radicals $RC(O)O_2$ with HO_2 radicals.

Rate constants of $RC(O)O_2$ with HO_2 radicals

Because both $CH_3C(O)O_2$ and HO_2 are doublets, ¾ of the collisions occur on a triplet surface and ¼ occur on a singlet surface. The fractions are included in the theoretical rate constants by means of the electronic partition functions. The triplet surface can lead to singlet $CH_3C(O)OOH$ (peracetic acid) and triplet O_2. This will be called path a. The singlet surface can lead to singlet $CH_3C(O)OH$ (the acid product discussed above) and singlet O_3 (path b) or to doublet $CH_3C(O)O$ and doublet HO_3, where the latter can dissociate to doublet OH, and triplet O_2 (path c). We studied all these paths. Intersystem crossing between the singlet and triplet surfaces is possible due to spin-orbit coupling, but spin-orbit coupling is expected to be small for light atoms like H, C, and O, and so we neglect it. The enthalpies of stationary points on the potential energy surface for the $CH_3C(O)O_2 + HO_2$ system are presented in Fig. 3a. Details of the theoretical calculation are provided in the Methods section. The pathways on the singlet surface (paths b and c) are relatively complex. As pointed out in previous work by Hasson et al.[32], the reactants first form a hydrotetraoxide (ROOOOH, AD) intermediate, which then decomposes to form $CH_3C(O)OH + O_3$ (path b) or $CH_3C(O)O + OH + O_2$ (path c).

The intermediates and enthalpies for $HC(O)O_2 + HO_2$ system are in Fig. 3b and are analogous to those of the $CH_3C(O)O_2 + HO_2$ system. The pathway on the triplet surface (path a) leads to performic acid and triplet O_2. The pathways on the singlet surface (path b and path c) form $HC(O)OH + O_3$ (path b) or $HC(O)O + OH + O_2$ (path c).

In addition to the pathways discussed above, we also considered the possibility of an intramolecular H-shift within the PC4 complex (i.e., the $RC(O)O(HO_3)$ adduct) to form PC3. Our quantum chemical calculations indicate that while such a pathway exists, but that its energy barrier is significantly higher (by approximately 10–12 kcal/mol) than that for direct dissociation into $RC(O)O + HO_3$. Consequently, the H-shift pathway is kinetically uncompetitive.

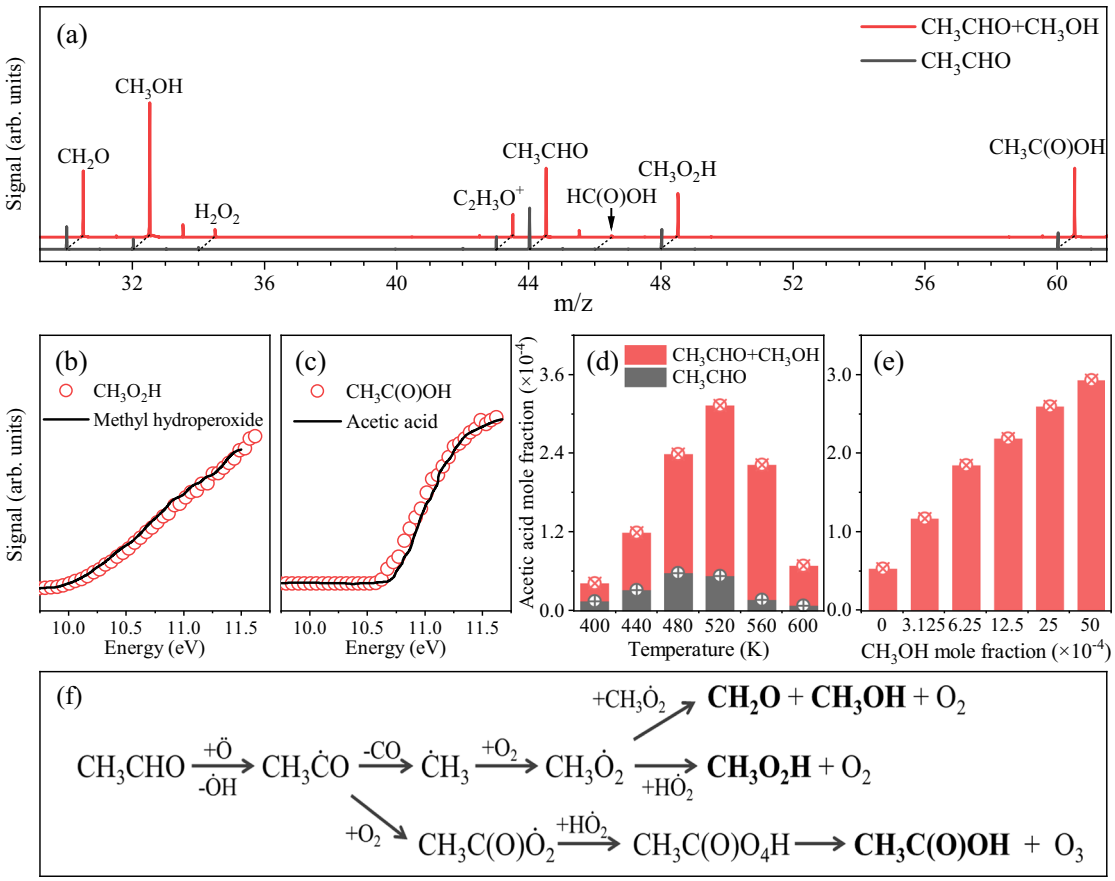

Fig. 2 | Cool-flame chemistry of CH_3CHO and CH_3OH + CH_3CHO. a Mass spectra of the cool-flame reactions of CH_3CHO and the CH_3OH + CH_3CHO mixture recorded by synchrotron vacuum ultraviolet photoionization mass spectrometry (SVUV-PIMS) at 520 K with a photon energy of 11.5 eV. Black line: the experimental spectra of the cool-flame reactions of CH_3CHO; Red line: the experimental spectra of the cool-flame reactions of CH_3OH + CH_3CHO. **b**, **c** CH_3O_2H and $CH_3C(O)OH$ product identifications by comparing the photoionization efficiency (PIE) spectra of methyl hydroperoxide[31] and acetic acid[28]. Red symbols: the experimental PIE spectra measured in this work; Black lines: the reference PIE spectra from the literature (methyl hydroperoxide[31] and acetic acid[28]). **d** The mole fraction of acetic acid formed in the cool-flame reaction of CH_3CHO in the temperature range of 400–600 K with or without CH_3OH addition. Black: experimental results for CH_3CHO system; Red: experimental results for CH_3OH + CH_3CHO system. The data points are also plotted with symbols. Source data are provided as a Source Data file. **e** The mole fraction of acetic acid formed by adding various amounts of CH_3OH to the reaction system of CH_3CHO at 520 K. The data points are also plotted with symbols. Source data are provided as a Source Data file. **f** Reaction pathway of the cool-flame reaction of acetaldehyde. The characteristic products (CH_2O, CH_3OH, CH_3O_2H and $CH_3C(O)OH$) formed through the pathway are highlighted in bold.

Hui et al.[33] measured the rate constants of the reactions on the triplet surface (path a) and the singlet surface (path b + path c). Using the above electronic calculations used for Fig. 3a, we calculated the temperature-dependent rate constants (see Methods), and the theoretical results are compared to the experiment in Fig. 3c, which shows good agreement for the negative temperature dependence. The calculated rate constants are too low, but only by factors of 3 (triplet) and 12 (singlet). Next, we used the measured rate constants to empirically adjust the electronic structure data by reducing the energies and enthalpies of all stationary points relative to reactants by 1.4 kcal/mol on the singlet surface and 0.5 kcal/mol on the triplet. (These adjustments are within the uncertainty of the electronic structure method[34,35].) Figure 3c shows that the adjusted rate constants agree well with the measurements; furthermore, Supplementary Fig. S2a shows that the adjusted calculations of the total rate constant are also in good agreement with several measurements of the total rate constant, which agree well with each other. Supplementary Fig. S2b shows that several measurements of the branching fractions agree well at 298 K. Figure 3d shows the branching fractions as functions of temperature from the adjusted calculations on $CH_3C(O)O_2$ + HO_2. As the temperature increases, the branching fraction of path a increases, while those for paths b and c decrease. Nevertheless, in the cool-flame zone of 500–800 K, the acetic acid formation pathway (path b) still accounts for 4–11% of the reaction.

There are no experimental results for $HC(O)O_2$ + HO_2. We again reduced the relative energies and enthalpies relative to reactants by 1.4 and 0.5 kcal/mol for the single and triplet, respectively. The resulting total rate constants are shown in Supplementary Fig. S3, and the branching fractions are in Fig. 3e. The branching fraction for organic acid formation again decreases with increasing of temperature. The formic acid formation pathway (path b) accounts for 3–15% of the branching fraction at 500–800 K.

The rate constant expressions in CHEMKIN format for the adjusted calculations on both systems are given in Supplementary Table S2.

Role of $RC(O)O_2$ and HO_2 in forming organic acids

The mole fraction of formic acid and acetic acid in the cool flames of nine typical hydrocarbon fuel systems (propane, *n*-butane, *n*-pentane, *iso*-pentane, *neo*-pentane, *n*-hexane, *n*-heptane, 1-hexene, and 1-heptene) were measured by SVUV-PIMS in the present work (see Methods section and Supplementary Table S3). To evaluate the contribution of the $HC(O)O_2$ + HO_2 and $CH_3C(O)O_2$ + HO_2 reactions to the formation of formic acid and acetic acid in the combustion of these fuels, the rate constants in Supplementary Table S2 were added to the NUIG[36,37]

https://doi.org/10.1038/s41467-025-67986-w

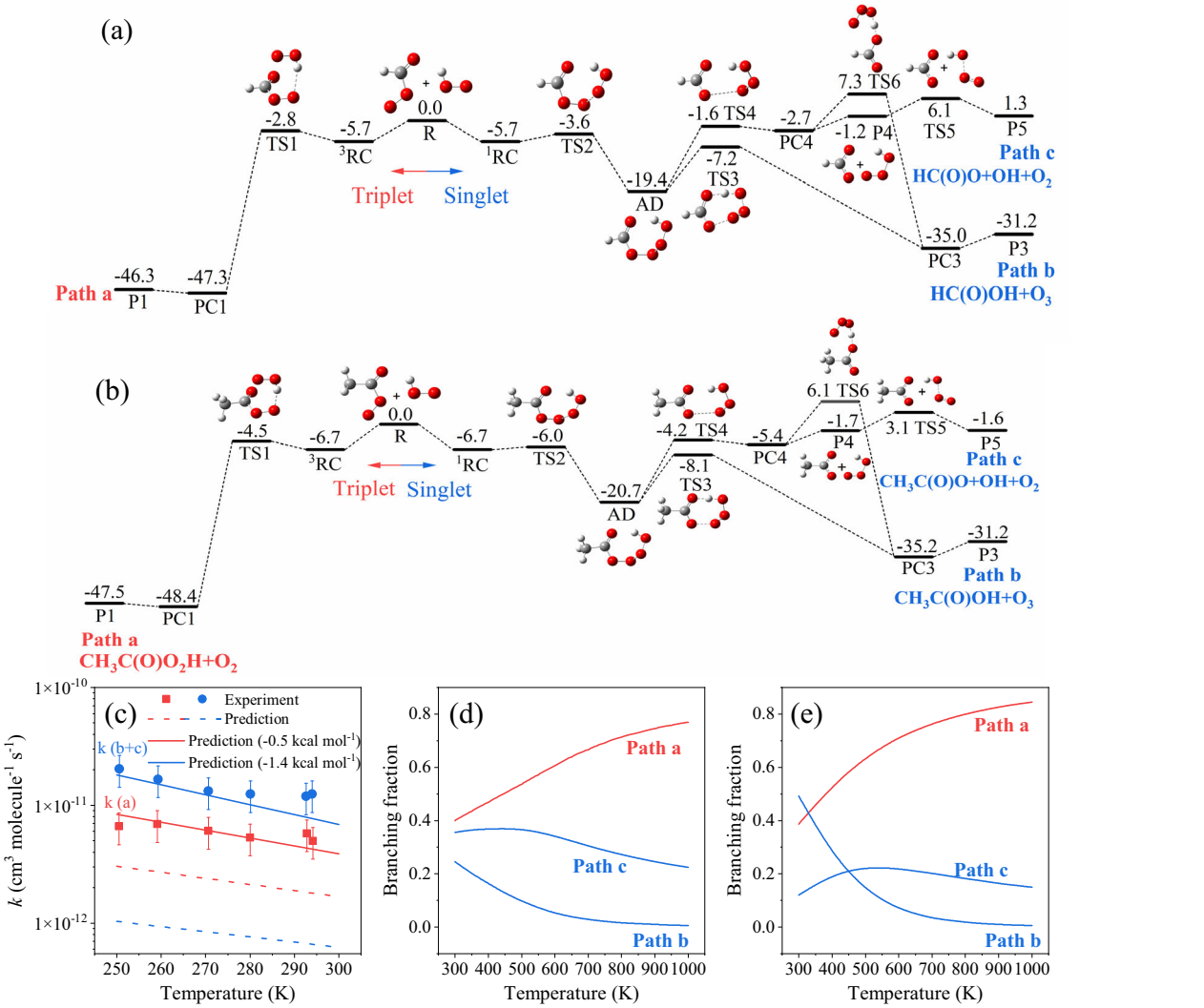

Fig. 3 | Energetics, rate constants and branching fractions of carbonyl peroxy radicals + HO_2 reaction. a, **b** Enthalpies of reactants, intermediates, transition states, and products of $CH_3C(O)O_2 + HO_2$ and $HC(O)O_2 + HO_2$ reactions calculated by CCSD(T)/CBS//B3LYP-D3(BJ)/def2-TZVP. Enthalpies are in kcal/mol at 0 K, at which temperature the enthalpy equals the sum of the potential energy and the zero point energy. Blue (Path b and Path c): singlet pathways; Red (Path a): triplet pathways. **c** Rate constants for the $CH_3C(O)O_2 + HO_2$ reaction: dashed lines represent unadjusted predictions (without energy corrections), solid lines represent adjusted predictions (with energy corrections applied), and symbols denote experimental data for singlet (blue) and triplet (red) pathways of the $CH_3C(O)O_2 + HO_2$ reaction, which from Hui et al.[28]. The adjustment refers to reducing the energies and enthalpies of all stationary points relative to reactants by 1.4 kcal/mol on the singlet surface and 0.5 kcal/mol on the triplet. Adjusted calculations of the branching fractions of the reaction pathways of $CH_3C(O)O_2 + HO_2$ (**d**) and $HC(O)O_2 + HO_2$ (**e**). Blue lines: the result of singlet pathways; Red lines: the result of triplet pathways.

model. Figure 4 shows that without these added reactions, the NUIG model significantly underestimates the mole fractions of formic acid and acetic acid, especially acetic acid. After adding the $HC(O)O_2 + HO_2$ and $CH_3C(O)O_2 + HO_2$ reaction pathways for formic acid and acetic acid, the model significantly improved the prediction of the mole fractions of these two organic acids. The model predictions suggest that the reaction pathways between carbonyl peroxy radical $RC(O)O_2$ and HO_2 radical are an important source of organic acid in cool-flame reactions.

We also considered the possibility that OH radicals, which are produced in the formaldehyde, acetaldehyde, and CH_3OH systems (e.g., via Pathway R2 and the decomposition of HO_3 radicals)—are significant contributors to organic acid formation by means of their direct reaction with carbonyl peroxy radicals $RC(O)O_2$ radicals, a pathway recently highlighted by Chen et al.[38] in the context of atmospheric chemistry. The key finding in this regard is that our formaldehyde and acetaldehyde systems, although they contained abundant $RC(O)O_2$ and OH radicals (e.g., via Pathway R2 and R3), produced only small amounts of organic acids. In contrast, in the CH_3OH and acetaldehyde + CH_3OH systems, increasing the concentration of HO_2 radicals (even in small amounts) markedly enhanced organic acid formation. This observation indicates that the reaction between $RC(O)O_2$ and HO_2 radicals, rather than the reaction between $RC(O)O_2$ and OH, is the primary source of organic acids in cool-flame reactions. To further validate this conclusion, we used a kinetic model to evaluate their contributions of the HO_2 reaction to acetic acid formation in the acetaldehyde system. In the kinetic model, the rate constant for the reaction $CH_3C(O)O_2 + HO_2 \rightarrow CH_3C(O)OH + O_3$ was that calculated in the present work. The kinetic model predicts that the mole fraction of acetic acid formed at 520 K and 760 Torr is 6.0×10^{-5}, in good agreement with the experimental value of $5.3 \pm 1.6 \times 10^{-5}$. This indicates the $CH_3C(O)O_2 + HO_2$ reaction is sufficient to account for the acetic acid formed. Adding the $CH_3C(O)O_2 + OH$ reaction would possibly increase acetic acid production beyond the experimental error bar, but a precise calculation is not possible because Chen et al. only calculated the rate constants in the temperature range 250–350 K at an

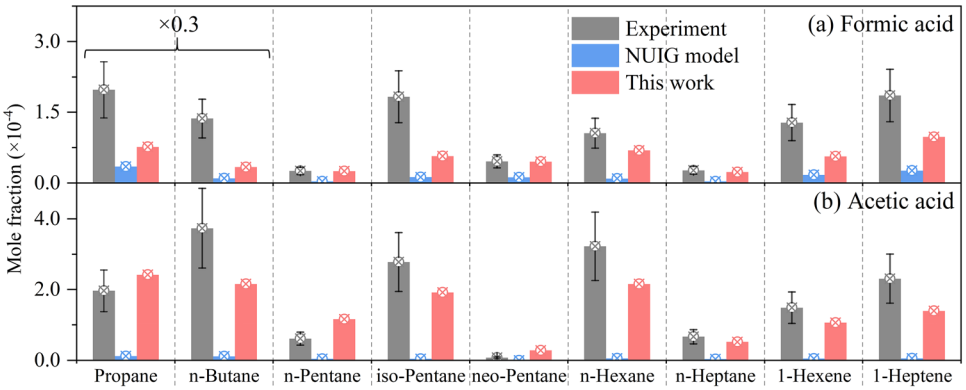

Fig. 4 | Formic and acetic acid formation during cool-flame oxidation of hydrocarbon fuels. Measured and calculated mole fractions of (**a**) formic acid and (**b**) acetic acid formed during the cool-flame reactions of nine typical hydrocarbon fuels: propane, *n*-butane, *n*-pentane, *iso*-pentane, *neo*-pentane, *n*-hexane, *n*-heptane, 1-hexene, and 1-heptene. Black (Experiment): experimentally measured mole fractions; Blue (NUIG model): the calculation results from the National University of Ireland Galway kinetics model[31,32]; Red (This work): the calculation results in this work after adding the $HC(O)O_2 + HO_2$ and $CH_3C(O)O_2 + HO_2$ pathways to the National University of Ireland Galway kinetics model[31,32]. The data points are also plotted with symbols. The error bars of the experimental measured mole fractions (±30%) are also given. Source data are provided as a Source Data file.

unspecified pressure. Further work to better understand the relative roles of the $CH_3C(O)O_2 + HO_2 \rightarrow CH_3C(O)OH + O_3$ pathway and the $CH_3C(O)O_2 + OH \rightarrow CH_3C(O)OH + O_2$ pathway under various conditions of temperature and pressure would be valuable.

We studied the cool-flame reactions of aldehydes, and we observed the direct formation of organic acids with the same carbon skeleton as the reacted aldehyde. We confirmed that the reaction of carbonyl peroxy radical with HO_2 radical is a missing source of organic acids during the cool-flame reactions of hydrocarbons. Adopting the newly obtained rate constants to combustion models at 500–800 K significantly improved the model prediction of organic acids. This work is useful not only to evaluate the emission potential of organic acids from different types of fuels, but also to predict the urban emission of organic acids, which is needed to investigate the climate effect of organic acids.

Methods

SVUV-PIMS experiments

Aldehyde cool-flame experiments were carried out in a jet-stirred reactor, and in-situ high-mass-resolution SVUV-PIMS was used to measure the species distribution in the reaction system. The H-atom abstraction reactions of aldehydes and methanol by active species and the subsequent O_2 addition reaction are effective methods for generating carbonyl peroxy $RC(O)O_2$ radicals and HO_2 radicals. Considering the temperature range (>400 K) involved in the cool-flame environment, the thermal decomposition of ozone is an ideal method to produce O atoms as the active species because (i) ozone thermal decomposition only produces O_2 and O atoms, and the interference introduced into the reaction system is limited[39] and (ii) the direct reaction between ozone and methanol/aldehydes is negligible[40]. Therefore, this work uses O atoms generated by ozone thermal decomposition as active species to produce carbonyl peroxy $RC(O)O_2$ radicals and HO_2 radicals.

We used this source of carbonyl peroxy $RC(O)O_2$ radicals and HO_2 radicals to study the cool-flame reactions of typical aldehydes (formaldehyde, acetaldehyde, propanal, *n*-butanal, *iso*-butanal, and benzaldehyde); the experimental details are provided in Supplementary Table S1.

We used SVUV-PIMS to measure the mole fractions of formic acid and acetic acid in the cool-flame reaction of nine typical hydrocarbon fuels in a jet-stirred reactor, including propane, *n*-butane, *n*-pentane, *iso*-pentane, *neo*-pentane, *n*-hexane, *n*-heptane, 1-hexene, and 1-heptene. These experimental results were used to evaluate the reaction of carbonyl peroxy $RC(O)O_2$ radical and HO_2 radical in the formation of formic acid and acetic acid. Experimental details are provided in the Supplementary Methods of Electronic Supplementary Information (ESI), with experimental conditions presented in Supplementary Table S3.

Quantum chemistry calculations

We used the *MSTor* software[41,42] and *Gaussian 16* software[43] for conformer searches to obtain the lowest-energy conformers. Optimized geometries, frequency analysis, and zero-point-energy calculations for all minima and transition states were performed using B3LYP-D3(BJ)/def2-TZVP; open-shell-singlet diradical structures were modelled using broken spin symmetry. The optimized geometries of all stationary points are provided in Supplementary Table S4. A vibrational-frequency scaling factor of 0.999 was used to correct the B3LYP-D3(BJ)/def2-TZVP frequencies to compute zero-point vibrational energies.

We performed single-point energy calculations of optimized structures with CCSD(T), and we used the cc-pVTZ and cc-pVQZ basis set to extrapolate these calculations to the complete basis set (CBS) limit[44]. T1 diagnostics were performed using CCSD(T)/cc-pVTZ calculations, and we found T1 values less than 0.02 for all closed-shell species and less than 0.045 for all open-shell species, implying that multireference effects are not strong[45,46].

All enthalpies are reported at 0 K, where the enthalpy is the sum of the potential energy and the zero-point energy.

Rate constant calculations

The temperature-dependent rate constants for the various reaction channels were determined by solving one-dimensional time-dependent master equations utilizing the Master Equation System Solver (MESS) program[47]. Reactions with energy barriers were modelled using conventional transition state theory with the rigid-rotor harmonic-oscillator assumption; tunnelling was considered by employing the one-dimensional (1-D) Eckart model in MESS. Barrierless reactions were modelled using phase space theory[48].

The bath gas was argon (Ar), and the Lennard–Jones (L-J) potential was employed for the energy-transfer calculations with parameters[49,50] $\sigma = 6.01$ Å and $\varepsilon = 464.1$ K for $HC(O)O_2$–HO_2 adducts, $\sigma = 6.15$ Å and $\varepsilon = 471.8$ K for $CH_3C(O)O_2$–HO_2 adducts, and $\sigma = 3.55$ Å and $\varepsilon = 116.2$ K for Ar. The energy transfer process was modelled using the single-parameter exponential down model, with $\langle \Delta E_{down} \rangle = 200(T/300)^{0.85}$ cm^{-1} for the average downward energy transferred per collision[51].

Rate constants for each reaction channel were obtained at atmospheric pressure in the temperature range of 250–1000 K. These rate constants were fitted to 3-parameter forms for the kinetics model; the parameters are in Supplementary Table S2.

Kinetics model and simulations

We started with the National University of Ireland Galway (NUIG) kinetics model[36,37]. This model contains the aldehyde + OH → organic acid pathway and the Korcek pathways of γ-KHPs, but those reactions are not sufficient to explain the formation of organic acids. We added all the reaction pathways and corresponding rate constants of $CH_3C(O)O_2 + HO_2$ and $HC(O)O_2 + HO_2$ systems to the NUIG model to evaluate the contribution of these reaction pathways to the prediction of formic acid and acetic acid in the cool-flame reactions of nine typical hydrocarbon fuels. All kinetics simulations were performed using the perfectly stirred reactor (PSR) module in the *Chemkin-Pro* software[52]. The experimental conditions in Supplementary Table S3 were used as input for the simulations. The steady-state simulation results are obtained by applying the transient solver, with the end time set to 80 seconds.

To evaluate the role of the $CH_3C(O)O_2 + OH$ reaction in acetic acid formation in the acetaldehyde cool-flame system, we incorporated the $CH_3C(O)O_2 + HO_2 \rightarrow CH_3C(O)OH + O_3$ reaction into the National University of Ireland, Galway (NUIG) kinetic model[36,37] to simulate acetic acid formation in acetaldehyde systems. The experimental measurement and simulated result are presented in the section on the role of $RC(O)O_2$ and HO_2 in forming organic acids.

Data availability

The data generated in this study are provided in the Supplementary Information/Source Data file, and the modified kinetic model (kinetic and thermodynamic files) are provided as Supplementary Data 1 and 2. Source/Supplementary data are provided with this paper and are also available at figshare (https://doi.org/10.6084/m9.figshare.30281779). Source data are provided with this paper.

References

1. Cong, Z., Kawamura, K., Kang, S. & Fu, P. Penetration of biomass-burning emissions from South Asia through the Himalayas: new insights from atmospheric organic acids. *Sci. Rep.* **5**, 9580 (2015).
2. Franco, B. et al. Ubiquitous atmospheric production of organic acids mediated by cloud droplets. *Nature* **593**, 233–237 (2021).
3. Millet, D. B. et al. A large and ubiquitous source of atmospheric formic acid. *Atmos. Chem. Phys.* **15**, 6283–6304 (2015).
4. Niu, Y., Li, X., Pu, J. & Huang, Z. Organic acids contribute to rainwater acidity at a rural site in eastern China. *Air Qual. Atmos. Health* **11**, 459–469 (2018).
5. Liu, N., Lei, J., Gao, W., Chen, H. & Xie, X. Combustion dynamics of large-scale wildfires. *Proc. Combust. Inst.* **38**, 157–198 (2021).
6. Liu, N. et al. Effect of slope on spread of a linear flame front over a pine needle fuel bed: experiments and modelling. *Int. J. Wildland Fire* **23**, 1087–1096 (2014).
7. Lei, J., Liu, N., Zhang, L. & Satoh, K. Temperature, velocity and air entrainment of fire whirl plume: A comprehensive experimental investigation. *Combust. Flame* **162**, 745–758 (2015).
8. Lei, J. et al. Experimental research on combustion dynamics of medium-scale fire whirl. *Proc. Combust. Inst.* **33**, 2407–2415 (2011).
9. Liu, N. et al. Global burning rate of square fire arrays: Experimental correlation and interpretation. *Proc. Combust. Inst.* **32**, 2519–2526 (2009).
10. Kawamura, K., Ng, L. L. & Kaplan, I. R. Determination of organic acids (C_1-C_{10}) in the atmosphere, motor exhausts, and engine oils. *Environ. Sci. Technol.* **19**, 1082–1086 (1985).
11. Zervas, E., Montagne, X. & Lahaye, J. Influence of fuel and air/fuel equivalence ratio on the emission of hydrocarbons from a SI engine. 1. *Experimental findings. Fuel* **83**, 2301–2311 (2004).
12. Zervas, E., Montagne, X. & Lahaye, J. Emission of specific pollutants from a compression ignition engine. Influence of fuel hydrotreatment and fuel/air equivalence ratio. *Atmos. Environ.* **35**, 1301–1306 (2001).
13. Zervas, E., Montagne, X. & Lahaye, J. Emission of alcohols and carbonyl compounds from a spark ignition engine. Influence of fuel and air/fuel equivalence ratio. *Environ. Sci. Technol.* **36**, 2414–2421 (2002).
14. Zervas, E., Montagne, X. & Lahaye, J. C_1–C_5 organic acid emissions from an SI engine: Influence of fuel and air/fuel equivalence ratio. *Environ. Sci. Technol.* **35**, 2746–2751 (2001).
15. Bock, N., Baum, M. M., Anderson, M. B., Pesta, A. & Northrop, W. F. Dicarboxylic Acid Emissions from Aftertreatment Equipped Diesel Engines. *Environ. Sci. Technol.* **51**, 13036–13043 (2017).
16. Li, T. et al. Emissions of carboxylic acids, hydrogen cyanide (HCN) and isocyanic acid (HNCO) from vehicle exhaust. *Atmos. Environ.* **247**, 118218 (2021).
17. Mayer, A. C. R. et al. Particulate Filters for Combustion Engines to Mitigate Global Warming. Estimating the Effects of a Highly Efficient but Underutilized Tool. *Emission Control Sci. Technol.* **10**, 10–21 (2024).
18. Agarwal, A. K., Singh, A. P. & Maurya, R. K. Evolution, challenges and path forward for low temperature combustion engines. *Prog. Energy Combust. Sci.* **61**, 1–56 (2017).
19. Yao, M. et al. A theoretical study on the effects of thermal barrier coating on diesel engine combustion and emission characteristics. *Energy* **162**, 744–752 (2018).
20. Xu, S., Zhu, R. S. & Lin, M. C. Ab initio study of the OH + CH_2O reaction: The effect of the OH··OCH_2 complex on the H-abstraction kinetics. *Int. J. Chem. Kinet.* **38**, 322–326 (2006).
21. Wu, X., Huang, C., Chai, J. & Zhang, F. Formation of Substituted Alkyls as Precursors of Peroxy Radicals with a Rapid H-Shift in the Atmosphere. *J. Phys. Chem. Lett.* **12**, 8790–8797 (2021).
22. Battin-Leclerc, F., Konnov, A. A., Jaffrezo, J. L. & Legrand, M. To Better Understand the Formation of Short-Chain Acids in Combustion Systems. *Combust. Sci. Technol.* **180**, 343–370 (2007).
23. Jalan, A. et al. New pathways for formation of acids and carbonyl products in low-temperature oxidation: the Korcek decomposition of γ-ketohydroperoxides. *J. Am. Chem. Soc.* **135**, 11100–11114 (2013).
24. Popolan-Vaida, D. M. et al. Formation of Organic Acids and Carbonyl Compounds in *n*-Butane Oxidation via γ-Ketohydroperoxide Decomposition. *Angew. Chem. Int. Ed. Engl.* **61**, e202209168 (2022).
25. Goldsmith, C. F., Burke, M. P., Georgievskii, Y. & Klippenstein, S. J. Effect of non-thermal product energy distributions on ketohydroperoxide decomposition kinetics. *Proc. Combust. Inst.* **35**, 283–290 (2015).
26. Wang, Z. D., Herbinet, O., Hansen, N. & Battin-Leclerc, F. Exploring hydroperoxides in combustion: History, recent advances and perspectives. *Prog. Energy Combust. Sci.* **73**, 132–181 (2019).
27. Zhu, L. et al. Ozone-assisted low-temperature oxidation of methane and ethane. *Proc. Combust. Inst.* **39**, 375–384 (2023).
28. Herbinet, O. et al. Experimental and modeling investigation of the low-temperature oxidation of *n*-heptane. *Combust. Flame* **159**, 3455–3471 (2012).
29. Dong, B. et al. Improving quantification of hydrogen peroxide by synchrotron vacuum ultraviolet photoionization mass spectrometry. *Combust. Flame* **242**, 112214 (2022).
30. Cool, T. A., Wang, J., Nakajima, K., Taatjes, C. A. & McIlroy, A. Photoionization cross sections for reaction intermediates in hydrocarbon combustion. *Int. J. Mass Spectrom.* **247**, 18–27 (2005).

31. Hu, Z. et al. Elucidating the photodissociation fingerprint and quantifying the determination of organic hydroperoxides in gas-phase autoxidation. *Proc. Natl. Acad. Sci. USA.* **120**, e2220131120 (2023).
32. Hasson, A. S., Kuwata, K. T., Arroyo, M. C. & Petersen, E. B. Theoretical studies of the reaction of hydroperoxy radicals (HO_2) with ethyl peroxy ($CH_3CH_2O_2$), acetyl peroxy ($CH_3C(O)O_2$), and acetonyl peroxy ($CH_3C(O)CH_2O_2$) radicals. *J. Photochem. Photobiol. A* **176**, 218–230 (2005).
33. Hui, A. O., Fradet, M., Okumura, M. & Sander, S. P. Temperature Dependence Study of the Kinetics and Product Yields of the HO_2+$CH_3C(O)O_2$ Reaction by Direct Detection of OH and HO_2 Radicals Using 2f-IR Wavelength Modulation Spectroscopy. *J. Phys. Chem. A* **123**, 3655–3671 (2019).
34. Peterson, K. A., Feller, D. & Dixon, D. A. Chemical accuracy in ab initio thermochemistry and spectroscopy: current strategies and future challenges. *Theor. Chem. Acc.* **131**, 1–20 (2012).
35. Zheng, J., Zhao, Y. & Truhlar, D. G. The DBH24/08 Database and Its Use to Assess Electronic Structure Model Chemistries for Chemical Reaction Barrier Heights. *J. Chem. Theory Comput.* **5**, 808–821 (2009).
36. El-Sabor Mohamed, A. A., Panigrahy, S., Sahu, A. B., Bourque, G. & Curran, H. J. An experimental and kinetic modeling study of the auto-ignition of natural gas blends containing C_1–C_7 alkanes. *Proc. Combust. Inst.* **38**, 365–373 (2021).
37. Panigrahy, S., Mohamed, A. A. E.-S., Wang, P., Bourque, G. & Curran, H. J. When hydrogen is slower than methane to ignite. *Proc. Combust. Inst.* **39**, 253–263 (2023).
38. Chen, H., Wang, S. & Wang, L. Reaction of the Acetyl Peroxy Radical and OH Radical as a Source of Acetic Acid in the Atmosphere. *ACS Earth Space Chem.* **8**, 2522–2531 (2024).
39. Sun, W. T., Gao, X., Wu, B. & Ombrello, T. The effect of ozone addition on combustion: Kinetics and dynamics. *Prog. Energy Combust. Sci.* **73**, 1–25 (2019).
40. Liu, B. et al. Ozone-assisted low temperature oxidation of methanol and ethanol. *Appl. Energy Combust. Sci.* **12**, 100085 (2022).
41. Zheng, J., Mielke, S. L., Clarkson, K. L. & Truhlar, D. G. MSTor: A program for calculating partition functions, free energies, enthalpies, entropies, and heat capacities of complex molecules including torsional anharmonicity. *Comput. Phys. Commun.* **183**, 1803–1812 (2012).
42. Zheng, J., Meana-Pañeda, R. & Truhlar, D. G. MSTor version 2013: a new version of the computer code for the multi-structural torsional anharmonicity, now with a coupled torsional potential. *Comput. Phys. Commun.* **184**, 2032–2033 (2013).
43. Frisch, M. J. et al. *Gaussian 16*, Gaussian, Inc., Wallingford CT, 2016.
44. Sivaramakrishnan, R. et al. Rate Constants for the Thermal Decomposition of Ethanol and Its Bimolecular Reactions with OH and D: Reflected Shock Tube and Theoretical Studies. *J. Phys. Chem. A* **114**, 9425–9439 (2010).
45. Rienstra-Kiracofe, J. C., Allen, W. D. & Schaefer, H. F. The $C_2H_5 + O_2$ Reaction Mechanism: High-Level ab Initio Characterizations. *J. Phys. Chem. A* **104**, 9823–9840 (2000).
46. Lee, T. J. & Taylor, P. R. A diagnostic for determining the quality of single-reference electron correlation methods. *Int. J. Quantum Chem.* **36**, 199–207 (1989).
47. Georgievskii, Y., Miller, J. A., Burke, M. P. & Klippenstein, S. J. Reformulation and solution of the master equation for multiple-well chemical reactions. *J. Phys. Chem. A* **117**, 12146–12154 (2013).
48. Forst, W. Unimolecular phase space theory rates by inversion of angular momentum-conserved partition function. *Phys. Chem. Chem. Phys.* **1**, 1283–1291 (1999).
49. Welty, J., Rorrer, G. L. & Foster, D. G. *Fundamentals of momentum, heat, and mass transfer*. John Wiley & Sons (2014).
50. Wang, H. et al. Kinetics of H-abstraction from isopentanol and subsequent β-dissociation and isomerization. *Combust. Flame* **246**, 112393 (2022).
51. Xing, L. et al. Global uncertainty analysis for RRKM/master equation based kinetic predictions: A case study of ethanol decomposition. *Combust. Flame* **162**, 3427–3436 (2015).
52. CHEMKIN-PRO 15092, Reaction Design, San Diego, 2009.

Acknowledgements

We are grateful to Prof. Hu Wang of Tianjin University for valuable discussions. This work is supported by the National Natural Science Foundation of China (W2411006 to Z.D.W.), National Key Research and Development Program of China (no. 2021YFA1601800 to Z.D.W.), CAS Project for Young Scientists in Basic Research (no. YSBR-028 to Z.D.W.), and the U.S. Department of Energy, Office of Science, Office of Basic Energy Sciences under Award (DE-SC0015997 to D.G.T.).

Author contributions

B.Z.L. and Z.D.W. designed the experiment; B.Z.L., B.D., Q.B.Z., W.Y.C., L.Y.W., and L.Z. carried out the experimental measurements; B.Z.L. performed the data analysis; B.Z.L., H.H.W., S.S.R., L.L.X., and D.G.T. carried out the theoretical analysis; B.Z.L., D.G.T., and Z.D.W. contributed to the preparation of the manuscript. D.G.T. and Z.D.W. supervised the project.

Competing interests

The authors declare no competing interests.

Additional information

Supplementary information The online version contains supplementary material available at https://doi.org/10.1038/s41467-025-67986-w.

Correspondence and requests for materials should be addressed to Donald G. Truhlar or Zhandong Wang.

Peer review information *Nature Communications* thanks Siddharth Iyer, and the other, anonymous, reviewer(s) for their contribution to the peer review of this work. A peer review file is available.

Reprints and permissions information is available at http://www.nature.com/reprints

Publisher's note Springer Nature remains neutral with regard to jurisdictional claims in published maps and institutional affiliations.

Open Access This article is licensed under a Creative Commons Attribution-NonCommercial-NoDerivatives 4.0 International License, which permits any non-commercial use, sharing, distribution and reproduction in any medium or format, as long as you give appropriate credit to the original author(s) and the source, provide a link to the Creative Commons licence, and indicate if you modified the licensed material. You do not have permission under this licence to share adapted material derived from this article or parts of it. The images or other third party material in this article are included in the article's Creative Commons licence, unless indicated otherwise in a credit line to the material. If material is not included in the article's Creative Commons licence and your intended use is not permitted by statutory regulation or exceeds the permitted use, you will need to obtain permission directly from the copyright holder. To view a copy of this licence, visit http://creativecommons.org/licenses/by-nc-nd/4.0/.

© The Author(s) 2025